AIAA JOURNAL
Vol. 30, No. 7, July 1992

Numerical Study of Juncture Flows

Chung-Lung Chen*
Rockwell International Science Center, Thousand Oaks, California 91360
and
Ching-Mao Hung†
NASA Ames Research Center, Moffett Field, California 94035

A computational study of laminar/turbulent and subsonic/supersonic horseshoe vortex systems generated by a cylindrical protuberance mounted on a flat plate is presented. Various vortex structures have been predicted and are discussed. For a low subsonic laminar flow, the number of computed vortex arrays increases with Reynolds number (with fixed incoming boundary-layer thickness), in agreement with experimental and previous numerical observations. The relationships among pressure extrema, vorticity, and the singular points in the flow structure on the plane of symmetry over the flat plate are studied. Mach number effects have also been investigated for laminar flow at one Reynolds number. The outermost singular point moves upstream when freestream Mach number increases. The size of the whole vortex structure increases dramatically due to shock-wave/boundary-layer interaction. The computed laminar horseshoe vortex systems start from a saddle point of attachment. In the case of a supersonic turbulent flow at a high Reynolds number, the computed results predict the same features as those indicated by the experimental results, such as the upstream shock-wave/boundary-layer interaction and the classical horseshoe vortex system starting from a saddle point of separation. The calculations provide details of the downstream wake/shock-wave interaction and the near wake tornadolike vortex structure. The overall flow topology is discussed.

Nomenclature

A = attachment
C_p = pressure coefficient
D = diameter of cylinder
d_1, d_2 = distance measured from the flat plate and cylinder
E = extremum of $p(x)$
H = height or semiheight of cylinder (clear from context)
M_∞ = freestream Mach number
N, N' = node and half-node, respectively
p = pressure
Re_D = Reynolds number based on cylinder diameter
S = saddle or separation (clear from context)
S' = half-saddle
u = velocity component in x direction
x, y, z = Cartesian coordinates (origin is at center of cylinder)
δ_i = incoming boundary-layer thickness
δ = cylinder-location boundary-layer thickness
ξ, η = vorticity components in x, y directions
θ = angle of separation or attachment
μ, μ_t = molecular and turbulence eddy viscosity

I. Introduction

THE juncture-flow study presented here is motivated by work such as the multibody Space Shuttle and turbine rotor/stator interactions. In the case of the multibody Shuttle, many struts connect the orbiter, the external tank, and the solid rocket booster. Studying the generic juncture-flow problem may help to understand the characteristics of this flow and thereby to learn how to optimize the grid distribution from a limited grid size allowance. In the case of the rotor/stator interaction, two-dimensional calculations can give a good prediction for the midspan; however, secondary flows in turbines significantly influence total pressure losses inside turbomachinery blade channels. These secondary flows are generated from the endwall boundary layers on the hub and casing of the machine.

Besides being applicable to these works, juncture flows are of importance in external aerodynamics (e. g., wing-body junctures, wing-pylon junctures), submarine conning tower flow, and applications in meteorology and geology. Thus it is worthwhile to study the generic juncture flow, which consists of a cylindrical protuberance mounted normal to a flat plate as shown in Fig. 1. Understanding this basic juncture-flow structure should help in dealing with the aforementioned applications.

Although numerous generic juncture-flow cases have been studied experimentally, such as those given in Refs. 1-8, the

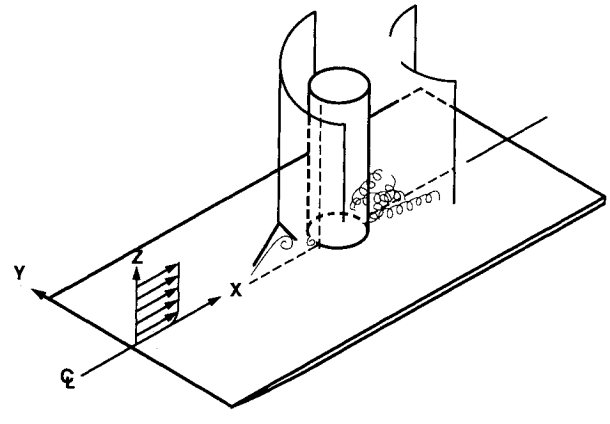

Fig. 1 Generic juncture flow (note: origin is at center of cylinder on plate surface).

Presented as Paper 91-1660 at the AIAA 22nd Fluid Dynamics, Plasma Dynamics, and Lasers Conference, Honolulu, HI, June 24-26, 1991; received June 28, 1991; revision received Sept. 16, 1991; accepted for publication Nov. 1, 1991.

*Member Technical Staff, Computational Fluid Dynamics Department. Member AIAA.
†Research Scientist, Computational Fluid Dynamics Branch. Associate Fellow AIAA.

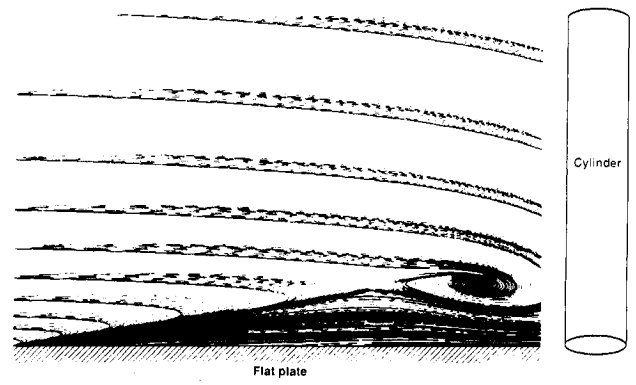

Fig. 2 Streamline pattern on the upstream plane of symmetry at $Re_D = 500$.

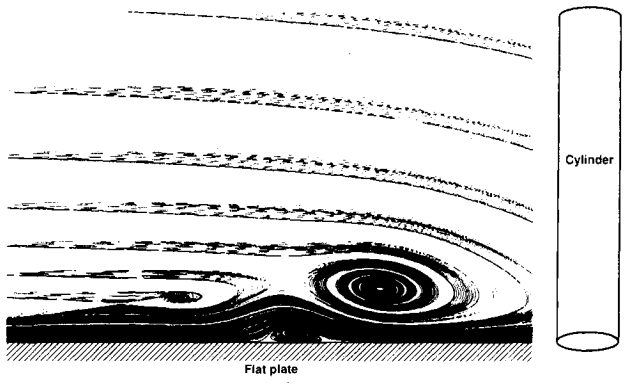

Fig. 3 Streamline pattern on the upstream plane of symmetry at $Re_D = 1500$.

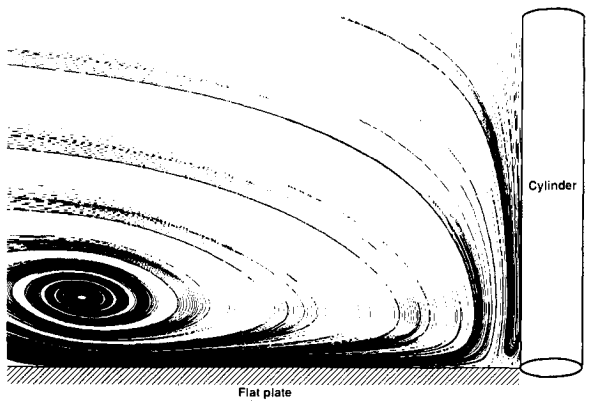

Fig. 4 Corner flow structure on the upstream plane of symmetry at $Re_D = 1500$.

associated complex horseshoe vortex system and wake structure remain a challenge for researchers trying to understand their intricacies. Relatively few computations have been conducted, and the studies have focused only on laminar low-speed juncture flow.[9-11] In the present study, low-speed laminar juncture flows are computed first to see the Reynolds number effect with the same incoming boundary-layer thickness, as done recently by Visbal.[10] Qualitative comparisons will be made among the computations, experimental observations, and analytic work. For incompressible flow, the relationships among pressure extrema, vorticity, and singular points in the flow structure will be discussed. This will be followed by a parametric study of the effect of freestream Mach number on the flow structure for laminar flow.

Another objective of this work is to compute the juncture flow when the incoming flow is turbulent and supersonic. A corresponding experimental work by Sedney and Kitchens[4] is available. The computational results will help shed light on the overall flow structure and on the near-wake region in particular. The difference in flow topology between the aforementioned cases will also be pointed out.

II. Numerical Approach

The equations solved here are the unsteady, three-dimensional, Reynolds-averaged, compressible, Navier-Stokes equations with an algebraic turbulence model used for closure. The computations are performed using the Unified Solution Algorithms (USA) code that is a finite volume, time-accurate, multizonal, Reynolds-averaged, Navier-Stokes solver featuring an implicit, upwind-biased scheme and total variation diminishing (TVD) discretization for high accuracy. The third-order spacial accuracy option is used in the present study. This code has been validated from low subsonic to hypersonic flows. Details on the USA series of codes can be found in Ref. 12.

The computations of low subsonic and supersonic laminar juncture flow are carried out first. The inflow boundary is located at 20 cylinder diameters away from the cylinder. For the subsonic flows ($M_\infty = 0.2, 0.6$), Blasius profiles are prescribed at the inflow boundary and are allowed to grow based on the distance from the leading edge of the flat plate (which is outside the computational domain). Blasius profiles are also used as initial conditions for the $M_\infty = 0.2$ case with $Re_D = 500$, the solution of which is used as initial condition for the $Re_D = 1500$ case. For the $M_\infty = 0.6$ case, the initial solution used is from the cases of $M_\infty = 0.2$. For the supersonic flow problem, the incoming boundary-layer profiles were obtained by solving a laminar flow past a flat plate. A space-marching version of the USA code was used for this purpose as well as for establishing the initial conditions. An outflow boundary condition is applied 30 diameters downstream of the cylinder. A no-slip adiabatic wall boundary condition is applied on the flat plate ($z = 0$) and cylinder surfaces, and the pressure gradient normal to the walls is set to zero. Symmetry conditions are applied at the top of the computational domain, corresponding to a cylinder sitting between two planes. Finally, the symmetry conditions are applied at the centerline ($y = 0$), and thus only half a cylinder is included in the computational domain. The vortex shedding in the wake is not of primary interest in the present study.

For the supersonic turbulent juncture-flow calculation, the space-marching version of the USA code was used again for setting up the inflow conditions and a modified Baldwin-Lomax turbulence model[13] was applied. The computed velocity profiles were prescribed at 10 diameters away from the juncture. This distance is twice as close to the juncture as that in the laminar-flow cases. The downstream far field is located 20 diameters downstream of the juncture. On the top boundary, zero flow gradients are applied. The rest of the boundary conditions are the same as those for the preceding case.

Although the laminar calculations use symmetry conditions (cylinder between two plates) and the supersonic turbulent calculation uses zero flow gradients at the top boundary of the computational domain, this study is applicable to any juncture flow where the height of the obstacle is large.

In the time-marching procedure, all of the computations were implemented in time-accurate fashion. A two-zone grid was used in this study: there is a half-O mesh around the cylinder and an H mesh extending into the wake region. The grid is then stacked up in the normal-to-the-plate direction. The half-O grid size used for the laminar flow calculations is $103 \times 157 \times 35$ (which is a sufficient grid size according to Ref. 10), and for the supersonic turbulent calculation it is $103 \times 77 \times 45$. The corresponding grid sizes of the H meshes are $10 \times 44 \times 35$ and $10 \times 44 \times 45$. The grid is clustered at the

cylinder and flat plate surfaces: the minimum grid spacing normal to the wall is $0.005D$ for laminar flow and $0.0005D$ for turbulent flow.

III. Results and Discussion

Two types of flows, laminar and turbulent, were computed. Laminar flows will be discussed in Sec. A for low Mach number with various Reynolds numbers and in Sec. B for various Mach numbers. A supersonic turbulent case will be discussed in Sec. C.

A. Laminar Juncture Flow for Two Reynolds Numbers

For the first case, the flow conditions for a cylinder with semiheight $H/D = 3.0$ attached between two plates are as follows: $M_\infty = 0.2$, the incoming boundary-layer thickness $\delta_i/D = 0.1$ at 20 diameters upstream of the cylinder juncture, and the Reynolds numbers based on the cylinder diameter (Re_D) are 500 and 1500. The flow conditions basically repeat Visbal's[10] but allow boundary-layer growth along the streamwise direction at the inflow boundary.

The computed streamline patterns at the upstream plane of symmetry are shown in Figs. 2 and 3. In spite of the fact that the boundary-condition treatment in the present work is not exactly the same as that in Ref. 10, the number of vortices increases from one to three as the Reynolds number increases, in agreement with Visbal's predictions and Baker's[1] observation qualitatively. The upstream outermost singular point is a saddle point of attachment on the flat plate, a half-nodal point

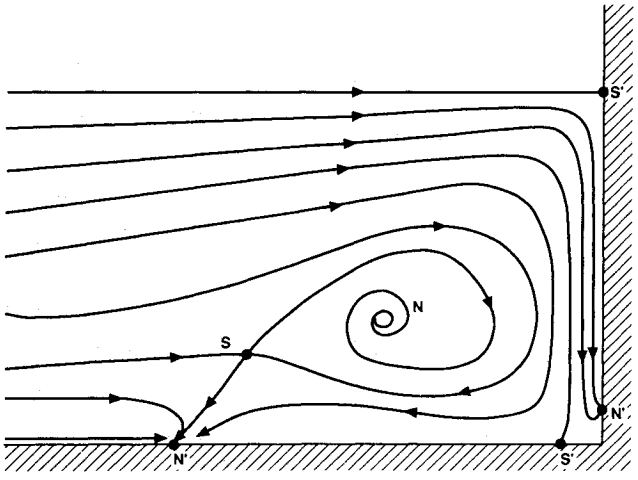

Fig. 5 Flow topology on the upstream plane of symmetry at $Re_D = 500$.

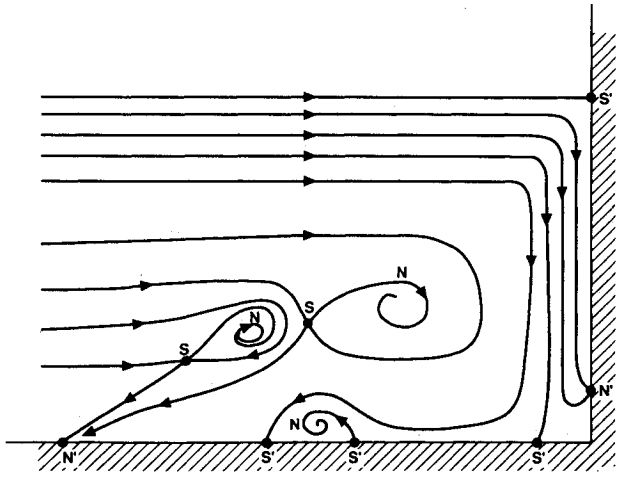

Fig. 6 Flow topology on the upstream plane of symmetry at $Re_D = 1500$.

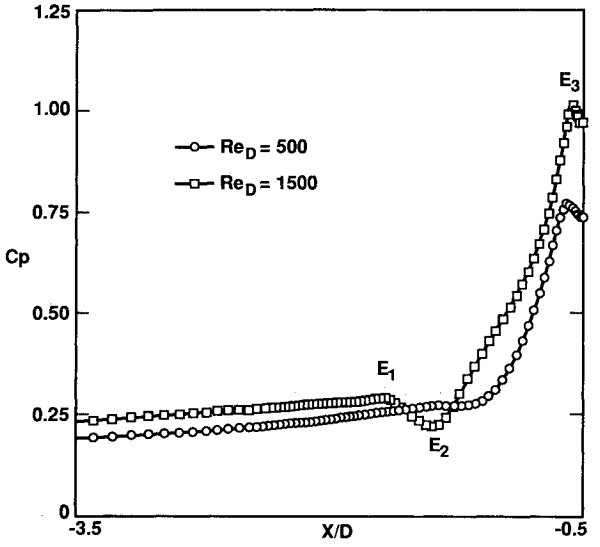

Fig. 7 Pressure coefficient profiles along the symmetry line on the upstream section of the flat plate.

in the x-z plane and a half saddle point in the y-z plane. The fluid enters this singular point as shown in Fig. 2. Interestingly enough, a similar pattern occurs near the corner of the cylinder as shown in Fig. 4. In fact, the existence of this type of singular point in symmetric incompressible laminar flow has been pointed out by Perry and Fairlie.[14] Their analytic work indicates that, if $\eta_x/\xi_y < 1$, the outermost saddle point is a point of attachment, whereas $\eta_x/\xi_y > 1$ will correspond to a point of separation. Here ξ and η are the vorticity components in the x and y directions, respectively. Furthermore, the flow will separate or attach from/to the wall when an angle $\theta = \tan^{-1}[\mu(\xi_y - 3\,\eta_x)/p_x]$ with respect to the $z = 0$ plane. The results presented here confirm the existence of a saddle point of attachment using this analysis. Consequently, a line with convergence of oil streak from both sides on the body surface in the experiment is not sufficient to be interpreted as a line of separation. (A detailed discussion of the saddle point of attachment can be found in Ref. 15.) The computed results in Figs. 2 and 3 also show that the saddle point of attachment moves upstream and the center of the closest primary vortex near the cylinder moves downward with increasing Reynolds number and the associated thinner boundary layer at the juncture location.

The flow topologies corresponding to Figs. 2 and 3, respectively, are sketched in Figs. 5 and 6. A topological rule has been developed for streamlines on a vertical plane cutting a surface that extends to infinity both upstream and downstream[16,17]:

$$(\Sigma_N + \tfrac{1}{2}\Sigma_{N'}) - (\Sigma_S + \tfrac{1}{2}\Sigma_{S'}) = 0 \qquad (1)$$

The singular points in this rule are defined as half-nodes (N'), half-saddles (S'), saddles (S), and nodes (N).[16,17] This rule has been used to describe the upstream plane of symmetry for an obstacle mounted on a wall in Ref. 16. With the inclusion of the singular point (half-saddle) at the leading edge of the flat plate, we have modified Eq. (1) as

$$(\Sigma_N + \tfrac{1}{2}\Sigma_{N'}) - (\Sigma_S + \tfrac{1}{2}\Sigma_{S'}) = -\tfrac{1}{2} \qquad (2)$$

This modified equation, referred to as the upstream rule, applies to the upstream plane of symmetry for a cylinder that is either sitting between two plates or mounted on a plate.

Topological rules are typically developed for the entire flowfield, including downstream of the obstacle. Applying upstream rules when the cylinder extends between two plates or when it extends well beyond the vortex structures created by the plate-cylinder juncture appears to be valid; however, diffi-

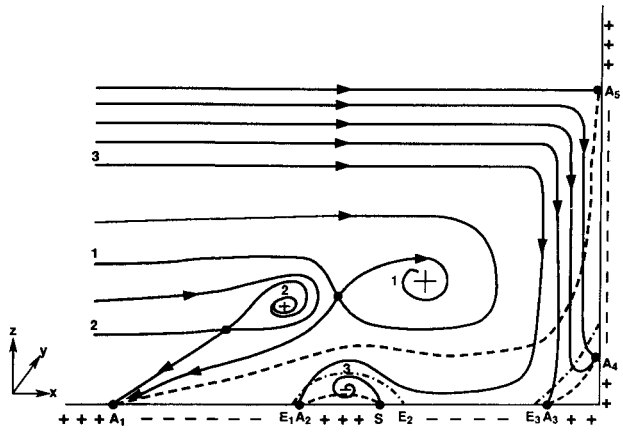

Fig. 8 Relation among pressure extrema, vorticity, and singular points; +, $\eta>0$; −, $\eta<0$; ---, line of $\eta=0$, − · −, line of $\partial\eta/\partial z=0$.

culties could arise when using these "upstream" rules with short obstacles.

Figure 5 shows that, after applying a symmetry boundary condition at the top plane, there are two foci, four half-nodes, two saddles, and five half-saddles (including one each at the leading edges of the plates). Thus, the sum of these equals $-\frac{1}{2}$. Similarly in Fig. 6, after applying symmetry conditions at the top plane, there are six foci, four half-nodes, four saddles, and nine half-saddles. Again, the sum of these equals $-\frac{1}{2}$.

The pressure coefficient on the line of symmetry along the flat plate is shown in Fig. 7. The peak pressure becomes higher with increasing Reynolds number. The results also agree qualitatively with Baker's[1] experimental observations. The pressure dip, or leveling out, occurs beneath the largest primary vortex near the cylinder, due to vortex-ground interaction. Again, experimental results[1,2] also show this feature.

For steady incompressible flow, the pressure extrema occurring on the symmetry line along the flat plate could be explained by examining the flow near the neighboring singular points. Figure 8, corresponding to Figs. 6 and 7, is used for this purpose. From the x-momentum equation it follows that the surface pressure extrema occur at $(1/\mu)(\partial p/\partial x)=\partial\eta/\partial z=\partial^2 u/\partial z^2=0$. A sufficient condition for the existence of a pressure extremum on the surface between two singular points is a change in sign of $\partial\eta/\partial z=\partial^2 u/\partial z^2$. The sign of $\partial\eta/\partial z$ will determine whether the extremum is a maximum or a minimum. The velocity component u is positive immediately above the outermost saddle point of attachment A_1, and $\partial u/\partial z=0.0$ at the singular point on the wall. Therefore, $\partial\eta/\partial z>0$ at A_1 [and it is a local minimum in the $u(z)$ profile]. Likewise, the velocity is negative immediately above the point A_2, that point corresponds to a local maximum in $u(z)$ and $\partial\eta/\partial z<0$ there. Consequently, at least one local pressure maximum exists between these two singular points, and the total number of pressure extrema will be odd unless an inflection in $p(x)$ occurs. Indeed, point E_1 in Fig. 7 is a corresponding pressure maximum between A_1 and A_2 but extremely close to A_2 (one grid point away). In addition, $\partial p/\partial x<0$ (i.e., $\partial\eta/\partial z<0$) just downstream of the leading edge of the flat plate; thus there is a local pressure minimum upstream of the saddle point of attachment. However, the changing of the sign is only a sufficient condition for the existence of a pressure extremum, not a necessary one. For instance, closer to the cylinder, at points S and A_3, $\partial\eta/\partial z$ does not change sign, which means that a pressure extremum may not exist or that an even number of pressure extrema may exist, providing that no inflection point in $p(x)$ does occur. In the present case of $Re_D=1500$, there is one local maximum (at E_3) and one local minimum (at E_2) between S and A_3, as shown in Fig. 7 (C_p plot). Usually, the singular point may not be at the location of pressure extremum. The pressure extremum will occur at the singular points only if $\partial^2 u/\partial z^2=0$ [or $u(z)$ immediately above the singular point is equal to zero] and the flow separates or attaches at 90 deg to the wall.

Another way to explain the existence of pressure extrema along the line of symmetry is from consideration of the vorticity field. Singular points in the pattern of skin-friction lines occur at isolated points on the surface where the vorticity vanishes. From the near-wall streamline direction we can determine the sign of the vorticity component η on the wall (positive and negative signs as seen in Fig. 8), which is the opposite of that of the corresponding vortices (primary and secondary). Consequently, there are lines of $\eta=0$ connecting "corresponding singular points" on the surface as shown in Fig. 8, since the vorticity field is continuous. (See Ref. 18 for discussions about the "corresponding singular points".) These singular points do not necessarily have to correspond to one separation and one attachment point. Note that over a common domain of x, between two neighboring lines of $\eta=0$, there exists at least one line of $\partial\eta/\partial z=0$. The intersections of these lines with the flat plate surface will correspond to the location of pressure extrema in $p(x)$ (e.g., points E_1, E_2, and E_3 in Figs. 7 and 8). They can be further evaluated as maxima or minima by investigating $\partial\eta/\partial z$ at the associated singular points as discussed in the preceding section. In fact, there is another locus line of $\eta=0$ that can be drawn from the leading edge of the flat plate through the freestream ($-\infty$) to the top

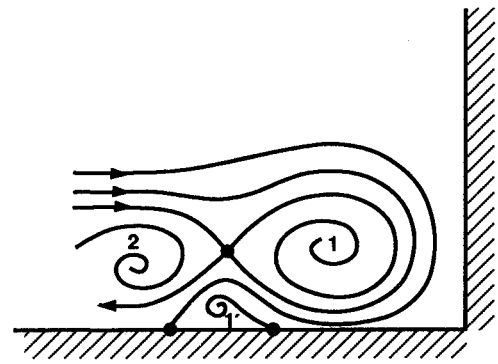

a) Jet-maze model

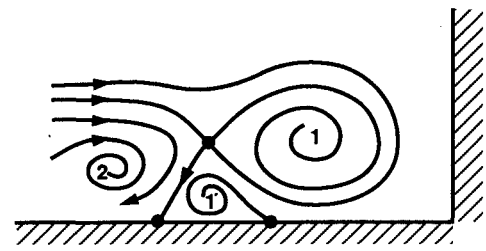

b) Stairstep model

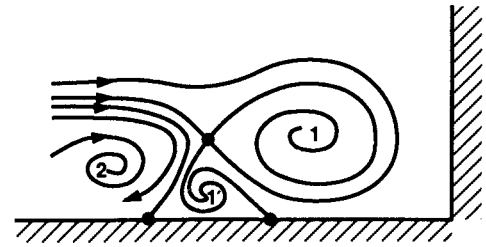

c) Alternative model

Fig. 9 Local connection among three vortices.

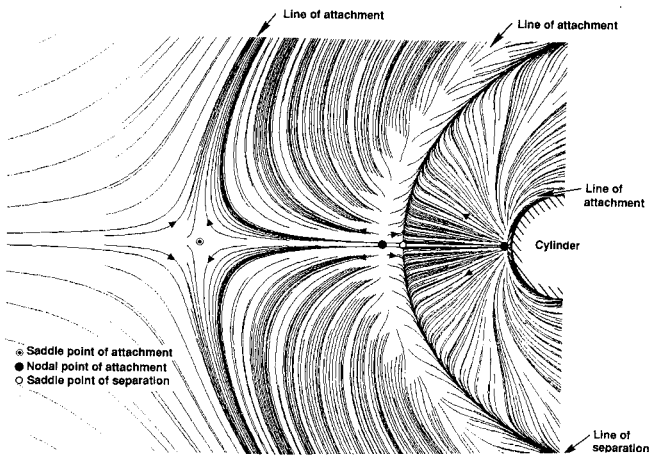

Fig. 10 Computed skin-friction line pattern on the surface of the flat plate at $Re_D = 1500$, $M_\infty = 0.6$.

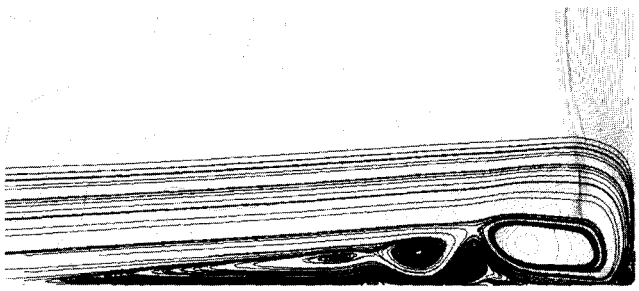

Fig. 11 Pressure contours and instantaneous streamline pattern ahead of the cylinder at $M_\infty = 2.0$.

symmetry plane. Consequently, another line of $\partial\eta/\partial z = 0$ between the top two lines of $\eta = 0$ intersects the flat plate and the intersection corresponds to a local pressure minimum upstream of the saddle point of attachment in the present results.

Finally, the upstream fluid is entrained by the vortices as seen in Fig. 8. One can realize how different an experimental interpretation of vortex structure would exist if smoke were released only at upstream layers 1, 2, and 3. Similarly, if grid resolution is not sufficient for the computation, a possible risk of missing details of the flow structure will be taken. The flow structure shown in Fig. 8 is different from the postulation of the jet-maze model or the stairstep model of Norman[5] used for interpretation of a different flow condition. Such flow conditions can cause quite a different flow structure. However, if we ignore the outermost portion and focus on the neighborhood of the two primary horseshoe vortices and the underneath secondary vortex, the result is the same as that of the jet-maze model shown in Fig. 9a. A local view of a stairstep model is shown in Fig. 9b. Another possible similar topology is shown in Fig. 9c; a small deviation of a stairstep model will create a structure seen in Fig. 9c. However, all of them have the same skin-friction line pattern.

B. Laminar Juncture Flow for Various Mach Numbers

For the second case, the configuration is the same as that of the first case with $Re_D = 1500$, but M_∞ is set to 0.6 and 2.0. For the case of $M_\infty = 0.6$, the streamline pattern on the upstream plane of symmetry is similar to the results in Fig. 3. The saddle point of attachment remains obvious but moves from about $x = -3.0D$ to $-3.5D$. The skin-friction line pattern on the flat plate is shown in Fig. 10. The degree of skin-friction line convergence is weaker for the outermost line of attachment than the line of secondary separation. Three types of singular points exist at the line of symmetry: two nodal points of attachment, one saddle point of separation, and one saddle point of attachment. The skin-friction line pattern shown here is the same as that of the classical four vortex system (two primary and two secondary vortices) shown by Sedney and Kitchens.[4] However, there are only three vortices seen on the plane of symmetry in Figs. 3 and 4. In fact, even if the outermost primary horseshoe vortex disappears, the skin-friction line pattern will remain unchanged. In addition, a saddle point on the plan view cannot indicate its flow direction normal to the plate, whereas a nodal point on the plane can, due to conservation of mass. Therefore, we conclude that it requires consolidating the plan view with the other views to understand the three-dimensional flow structure.

Pressure coefficient contours and flow structure for flow at $M_\infty = 2.0$ are shown in Fig. 11. There is a bifurcated shock structure ahead of the cylinder, and some minor flow unsteadiness has been noticed. The number of horseshoe vortices increases to three (and three secondary vortices), and the outermost singular point ahead of the cylinder occurs farther upstream than in all of the other cases. The height of the whole vortex array also increases dramatically. In addition, the outermost line of convergence around the shoulder of the cylinder is about twice the upstream separation distance. This is quite different from all of the other cases just discussed, in which the side distance of outermost line of attachment is slightly larger than the upstream distance. All of this is due to the strong shock/boundary-layer interaction. In this case, al-

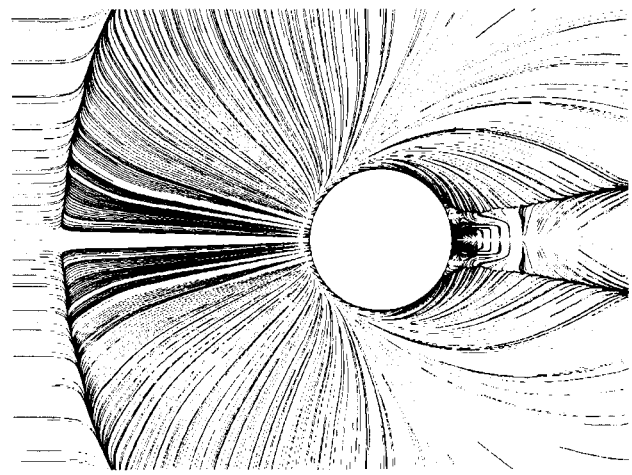

a) Computation

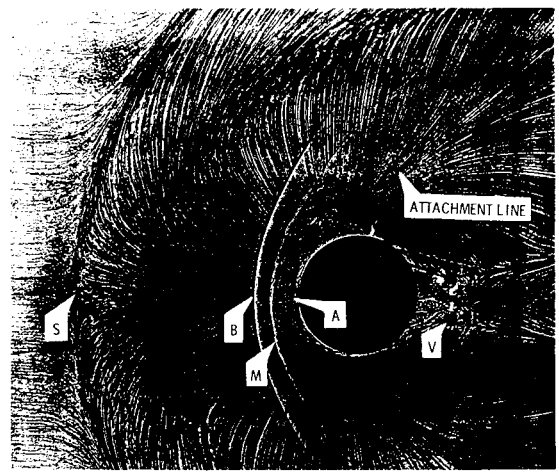

b) Experiment (Sedney &Kitchens)

Fig. 12 a) Computed skin-friction line pattern on the surface of the flat plate: $Re_D = 7.35 \times 10^5$, $M_\infty = 2.5$, and $\delta = 2.2$ cm; b) experimental oil-flow pattern on the flat plate: S—primary separation, B—bow shock, M—Mach stem, A—attachment line, V— vortex core; (attachment line originates at point A).

though the outermost singular point on the flat plate remains the saddle point of attachment, it is so close to its closest free saddle point that the structure of conventional spiral separation becomes the dominant feature, and the grid resolution may become insufficient to determine whether two or one singular points exist there. However, when these singular points become so close to each other, it is academic rather than practical to distinguish between them.

C. Supersonic Turbulent Juncture Flow

The third case discussed here is that of a supersonic turbulent incoming flow at $M_\infty = 2.5$, $Re_D = 7.35 \times 10^5$. A circular cylinder of diameter $D = 3.81$ cm and height $H = 10.16$ cm is bolted to the window of a supersonic wind tunnel where the turbulent boundary-layer thickness is $\delta = 2.2$ cm. The experimental work was done by Sedney and Kitchens.[4] The turbulence model used in the computation is a modified Baldwin-Lomax model[13] with Goldberg's backflow model[19] invoked in backflow regions. For multiple surfaces, the eddy viscosity is blended using a distance function: $\mu_t = (\mu_1/d_1 + \mu_2/d_2)/\sqrt{1/d_1^2 + 1/d_2^2}$ where d_1 and d_2 are the distances measured from the flat plate and the cylinder. Only the half-cylinder case is computed to reduce the computational effort. Since the Mach number is above one, the wake characteristics behind the circular cylinder change from periodic shedding at low speed to a quasisteady necked wake. The approximation of computing a half-cylinder rather than a full cylinder seems to be acceptable.

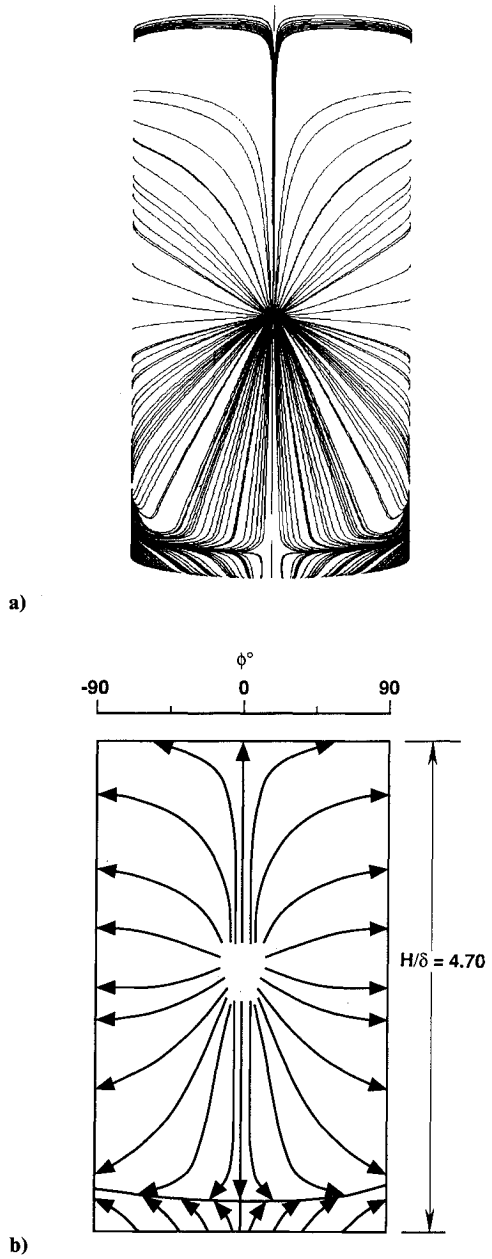

Fig. 13 a) Computed skin-friction line pattern on the front surface of the flat plate: $Re_D = 7.35 \times 10^5$, $M_\infty = 2.5$, and turbulent boundary layer with $\delta = 2.2$ cm; b) sketch of large protuberance surface flow pattern of Ref. 4.

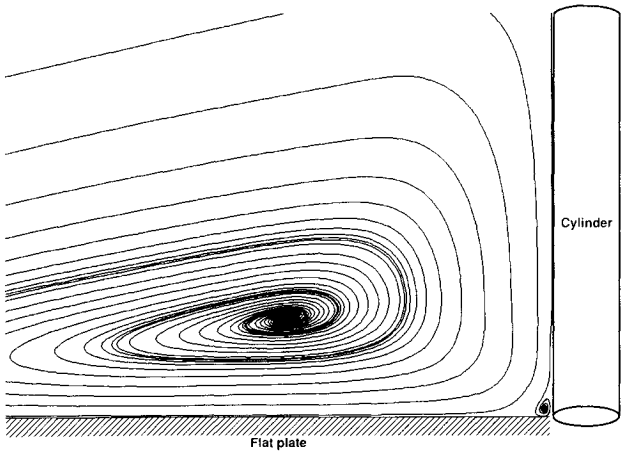

Fig. 14 Streamline pattern on the upstream plane of symmetry; flow conditions are same as those of Fig. 12.

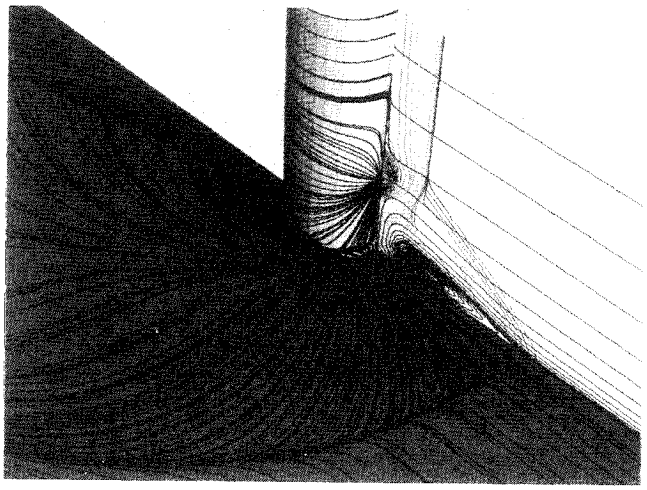

Fig. 15 Overall flow structure of the juncture flow at $Re_D = 7.35 \times 10^5$, $M_\infty = 2.5$, and $\delta = 2.2$ cm.

The computed skin-friction lines and streamlines are shown in Figs. 12a, 13a, and 14, which correspond to top view, front view, and upstream plane of symmetry, respectively. Figure 15 is a combination of Figs. 12–14. The flow separates from the wall at the upstream outermost singular point shown in Fig. 15. The character of the upstream saddle point has changed from one of attachment, as in the preceding cases, to one of separation.

The corresponding views of available experimental results are shown in Figs. 12b and 13b. The computed results seen in Fig. 12a are very similar to the experimental oil-flow pattern in Fig. 12b. The upstream saddle point of separation on the plane of symmetry at a distance is about 1.9 diameters upstream of the cylinder according to the experimental measurement. The corresponding computed saddle point is located at 1.78 diameters upstream of the cylinder. Since there is a slight amount of geometrical magnification in the images on the shadowgraph because of the diverging light from the spark source, the error can amount to 5%.[4] Because the local grid

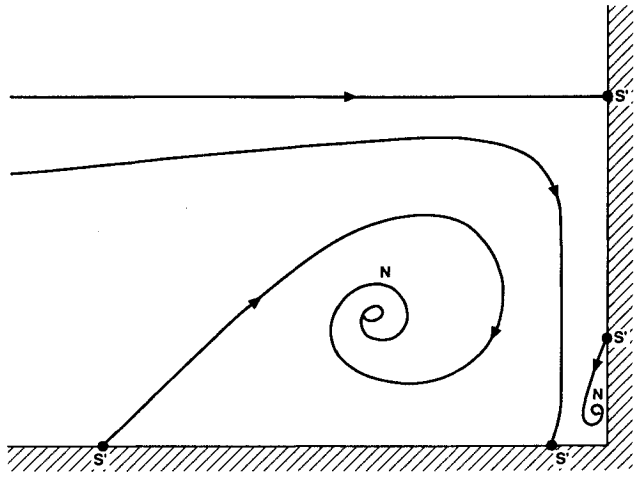

Fig. 16 Flow topology on the upstream plane of symmetry.

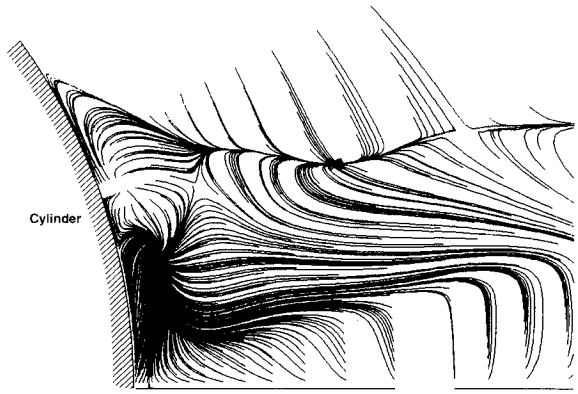

Fig. 17 Close view of skin-friction line pattern at the near-wake region.

spacing in the streamwise direction at the saddle-point location is about 0.2 diameter and a simple turbulence model is used, the agreement with the experiment is very encouraging. This saddle point of separation can be identified clearly in Fig. 15, in which the primary separation line merges and passes around and then goes downstream of the cylinder. Looking closely in the vicinity of the juncture, there exists a counter-rotating vortex seen in the enlargement of the particle trace in the symmetry plane (Fig. 14). In contrast with the corner flow structure in Fig. 4, the saddle point on the cylinder has also changed from one of attachment to one of separation. A nodal point of attachment (looking at the top view of the flat plate in Figs. 12 and 15) is located along the line of symmetry just ahead of the cylinder/wall junction. One skin-friction line passes from the attachment node to the saddle point of separation whereas others fan out from the attachment point. Two singular points are seen in the front view of the cylinder surface in Fig. 13 (a nodal point of attachment and a saddle point of separation). The center of the nodal point of attachment is determined by numerical integration of the velocity field in the negative time sense. A computed pressure peak is observed close to this nodal point. The skin-friction line pattern qualitatively agrees with a sketch of experimental results for a "large protuberance" (Fig. 13b), defined as a cylinder height larger than 2δ. A quantitative comparison cannot be made because the flow conditions and cylinder height are different in the experiment and in the computation, and zero flow gradients are assumed at the top of the computational boundary. The computed flow topology at the upstream plane of symmetry is sketched in Fig. 16. The difference between Fig. 16 and Fig. 5 is clear; however, checking the numbers of the singular points, there are five half-saddles (including the one at the leading edge of the flat plate) and two nodes, so that the topology index rule is again satisfied [see Eq. (2)]. The bifurcated shock structure ahead of the cylinder in the symmetry plane is also shown in Fig. 15 by the pressure coefficient contours superimposed with the streamlines. The highest pressure on the cylinder surface at the plane of symmetry is located behind the Mach stem (the rear leg of the lambda shock), close to the triple point and the nodal point of attachment in Fig. 13a. It can be found by following the superimposed streamline in Fig. 15. The clockwise spiraling primary vortex induces low pressure spots on the cylinder and the flat plate. This pressure dip can also be found in the laminar horseshoe vortex system. The overall flow features ahead of the cylinder are very similar to those of a blunt fin flow calculation by Hung and Buning[20] even though the geometry and flow conditions are not the same. Besides the observed flow shock ahead of the cylinder, another oblique shock is observed at the wake region due to flow overexpansion around the cylinder.

The near-wake topology based on our computed results (see a close view in Fig. 17) is shown at the top half of Fig. 18 and is compared with the Peake and Tobak[21] postulate (based on Fig. 12b) sketched in the bottom half of the figure. Three main nodes are seen in the wake: besides one nodal point of attachment at the centerline of the wake, a focus located closest to the cylinder "erupts" as a spiral filament into the flow, and another node is centered at the roll-up of the adjacent dividing surface that proceeds downstream. The two topologies are very similar to each other; the few minor differences are due mainly to the limited resolution of both the experimental data and the computation. One difference is that the present results include three extra singular points near the cylinder surface. Two are half-saddles and one is a full node. Another difference is that the computed node on the downstream separation line is a nodal point of separation with a tangent line along the separation line, whereas Peake and Tobak[21] refer to this node (dark dot in Fig. 12b) as a focus. Due to the lack of resolution in the experimental observations in the near wake (Fig. 12b), it is hard to judge which interpretation is closer to the experimental results. A focus (spiral node) may have been distorted into a nodal point due to insufficient grid resolution in the

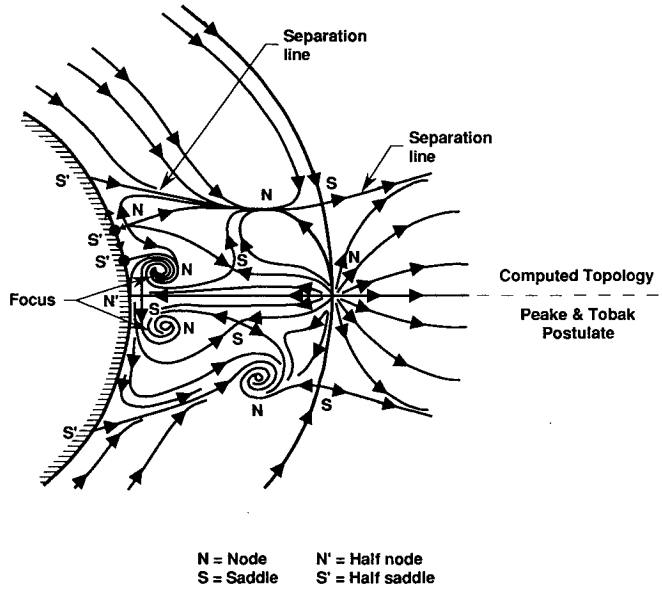

Fig. 18 Flow topology at the near-wake region.

computation. Nevertheless, the global near-wake flow structure predicted by the computation agrees with the experimental one.

On a two-dimensional plane cutting a three-dimensional, simply connected body immersed in a flow that is uniform far upstream, another topology rule applies,[16]

$$(\Sigma_N + \tfrac{1}{2}\Sigma_{N'}) - (\Sigma_S + \tfrac{1}{2}\Sigma_{S'}) = -1 \qquad (3)$$

The topology on a plane just above the flat plate must satisfy this rule, and it does (see Figs. 12 and 18), since $S = 1$, $S' = 1$, and $N = 1$ ahead of the cylinder, and $S = 5$, $S' = 6$, $N = 7$, and $N' = 1$ in the wake.

IV. Conclusions

A numerical study was done on both laminar and turbulent horseshoe vortex systems generated by flow past a cylindrical protuberance mounted on a flat plate. A qualitative comparison was made with available experimental data, and the results are very good. The overall flow topology and the topology index rules associated with juncture flow have been studied and analyzed.

The upstream outermost singular point can be either a saddle point of attachment or a saddle point of separation, depending on flow conditions. The skin-friction line pattern provides only two-dimensional flow information about the flow structure; to understand the entire flow structure, other views thereof are required.

In the case of a low subsonic laminar flow, the number of vortex arrays increases with increasing Reynolds number (with fixed incoming boundary-layer thickness), in agreement with both experimental and other numerical observations. As the Reynolds number increases, the peak pressure along the line of symmetry on the flat plate also increases. For incompressible flow, the location of pressure extrema at the line of symmetry on a flat plate associated with singular points and vorticity field has been examined.

In the case of a parametric study of the effect of freestream Mach number on the laminar flow structure, the results indicate the importance of Mach number on the flow topology. The outermost singular point moves upstream as the freestream Mach number increases. When a bifurcated shock structure occurs in the case of the Mach 2.0 flow, the number of vortices, as well as the size of the entire flow vortex structure, increases dramatically due to a shock-wave/laminar boundary-layer interaction. Furthermore, the conventional horseshoe vortex separation becomes the dominant flow feature near the outermost saddle point of attachment because the closest free saddle point moves very close to it.

In the case of a supersonic turbulent flow at high Reynolds number, the computed results provide the main features of this complex juncture flow in agreement with experimental results, such as the upstream shock-wave/boundary-layer interaction and the classical horseshoe vortex system that is starting from a saddle point of separation. The calculation provides details of the near-wake tornadolike vortex structure and the downstream wake/shock-wave interaction.

Overall, these results demonstrate that when a simple strut is introduced into the multibody Space Shuttle in ascent, a complex flowfield results as a consequence.

Acknowledgments

The first author of this work was sponsored by Rockwell IR&D, and all of the computations were performed on the Numerical Aerodynamic Simulation system.

References

[1]Baker, C. J., "The Laminar Horseshoe Vortex," *Journal of Fluid Mechanics,* Vol. 95, Pt. 2, 1979, pp. 347–367.

[2]Baker, C. J., "The Turbulent Horseshoe Vortex," *Journal of Wind Engineering and Industrial Aerodynamics,* Vol. 6, No. 11–12, 1980, pp. 9–23.

[3]Baker, C. J., "The Position of Points of Maximum and Minimum Shear Stress Upstream of Cylinders Mounted Normal to Flat Plates," *Journal of Wind Engineering and Industrial Aerodynamics,* Vol. 18, No. 3, 1985, pp. 263–274.

[4]Sedney R., and Kitchens, C. W., "The Structure of Three-Dimensional Separated Flows in Obstacle, Boundary-Layer Interactions," AGARD-CP-168, No. 37, May 1975.

[5]Norman, R. S., "On Obstacle Generated Secondary Flows in Laminar and Transition to Turbulence," Ph.D. Thesis, Illinois Inst. of Technology, Chicago, IL, Dec. 1972.

[6]Pierce, F. J., and Tree, I. K., "The Mean Flow Structure on the Symmetry Plane of a Turbulent Juncture Vortex," *Journal of Fluids Engineering,* Vol. 112, No. 1, 1990, pp. 16–20.

[7]Eckerle, W. A., and Langston, L. S., "Horseshoe Vortex Formation Around a Cylinder," *Journal of Turbomachinery,* Vol. 109, No. 2, 1987, pp. 278–285.

[8]Angui, J., and Andreopoulos, J., "Experimental Investigation of a Three-Dimensional Boundary Layer Flow in the Vicinity of an Upright Wall Mounted Cylinder," AIAA Paper 90-1545, June 1990.

[9]Kaul, U. K., Kwak, D., and Wagner, C., "A Computational Study of Saddle Point Separation and Horseshoe Vortex System," AIAA Paper 85-0182, Jan. 1985.

[10]Visbal, M. R., "Numerical Investigation of Laminar Juncture Flows," AIAA Paper 89-1873, June 1989.

[11]Briley, W. R., Buggelin, R. C., and McDonald, H., "Solution of the Three-Dimensional Navier-Stokes Equations for a Steady Laminar Horseshoe Vortex Flow," AIAA Paper 85-1520, July 1985.

[12]Chakravarthy, S. R., and Osher, S., "Computing With High-Resolution Upwind Schemes for Hyperbolic Equations," *Proceedings of the 1983 AMS-SIAM Summer Seminar on Large-Scale Computations in Fluid Mechanics, Lectures in Applied Mathematics,* Vol. 22, American Mathematical Society, Providence, RI, 1985.

[13]Ramakrishnan, S., and Goldberg, U., "Numerical Simulation of Swept Shock/Boundary-Layer Interactions," AIAA Paper 90-5234, Oct. 1990.

[14]Perry, A. E., and Fairlie, B. D., "Critical Points in Flow Patterns," *Advances in Geophysics,* Vol. 18B, Academic, New York, 1979, pp. 299–315.

[15]Hung, C. M., Sung, C. H., and Chen, C. L., "Computation of Saddle Point of Attachment," AIAA Paper 91-1713, June 1991.

[16]Tobak, M., and Peake, D. J., "Topology of Two-Dimensional and Three Dimensional Separated Flows," AIAA Paper 79-1480, July 1979.

[17]Hunt, J. C. R., Abell, C. J., Peterka, J. A., and Woo, H., "Kinematical Studies of the Flows around Free or Surface-Mounted Obstacles; Applying Topology to Flow Visualization," *Journal of Fluid Mechanics,* Vol. 86, Pt. 1, 1978, pp. 179–200.

[18]Hung, C. M., "Computation of Navier-Stokes Equations for Three-Dimensional Flow Separation," NASA TM 102266, Dec. 1989.

[19]Goldberg, U. C., "Separated Flow Treatment with a New Turbulence Model," *AIAA Journal,* Vol. 24, No. 10, 1986, pp. 1711–1713.

[20]Hung, C. M., and Buning, P. G., "Simulation of Blunt-Fin-Induced Shock-Wave and Turbulent Boundary-Layer Interaction," *Journal of Fluid Mechanics,* Vol. 154, May 1985, pp. 163–185.

[21]Peake, D. J., and Tobak, M., "Three-Dimensional Interactions and Vortical Flows with Emphasis on High Speeds," AGARD-AG-252, July 1980.